A coupled-mode-theory formulation for periodic multi-element metasurfaces in the presence of radiation losses ⊘

Maria-Thaleia Passia ✉ iD ; Traianos V. Yioultsis iD ; Emmanouil E. Kriezis iD

View Online   Export Citation   CrossMark

A coupled-mode-theory formulation for periodic multi-element metasurfaces in the presence of radiation losses

View Online   Export Citation   CrossMark

Maria-Thaleia Passia,[a)] (ID) Traianos V. Yioultsis, (ID) and Emmanouil E. Kriezis (ID)

AFFILIATIONS

School of Electrical and Computer Engineering, Aristotle University of Thessaloniki, Thessaloniki, Greece

[a)]Author to whom correspondence should be addressed: passiamg@ece.auth.gr

ABSTRACT

We derive a coupled-mode theory (CMT) formulation for the fast analysis of periodic multi-element metasurfaces in the presence of radiation losses. Full-wave simulations of periodic multi-element metasurfaces are very time- and memory-consuming, especially as the size and complexity of the metasurface increase. The CMT formulation provides a considerably faster and efficient alternative. It results in a small system of equations with size equal to the number of supported resonator modes in the frequency range of interest, allowing to calculate the resonator mode amplitudes and, consequently, the metasurface response. Subsequently, we systematically derive analytical closed-form expressions for the coupling coefficients between two weakly coupled resonators in the presence of radiation losses and incorporate them into the CMT model, which is found important for the accurate description of the metasurface, while also providing insight into the underlying physics of complex metasurfaces. We validate the proposed formulation on benchmark examples of both metal- and dielectric-based metasurface absorbers (MSAs) by comparing the CMT results to spectral FEM simulations of the composing supercell. To further demonstrate the potential of the proposed formulation, as a proof of concept, we use the CMT to synthesize a larger optimized periodic multi-element MSA. A comprehensive comparison to full-wave FEM simulations of the composing supercell is included in terms of time and computational requirements, which shows that our method provides a valuable and efficient alternative solver for synthesizing complex metasurfaces.

I. INTRODUCTION

Over the past years, metasurfaces have gained considerable interest, as they are the two-dimensional extension of the well-established electromagnetic metamaterials[1] and offer a planar and lightweight alternative to bulky electromagnetic devices.[2] Metasurfaces are capable of controlling and efficiently guiding propagating waves by engineering the properties of individual resonant elements. Although uniform metasurfaces have been used in several applications,[3] periodic multi-element designs have gained increasing interest, as they offer greater design flexibility. Periodic multi-element metasurfaces are synthesized by periodically repeating a combination of several resonators, which is commonly referred to as a supercell. The supercell consists of an arrangement of non-uniform resonators. The resonators may be of different shapes or sizes, each having different electromagnetic properties. Periodic multi-element metasurfaces are used to obtain a

broadband or multiband response, acting as absorbers or filters, as they combine multiple elements, each resonating at a different frequency.[4–6] Periodic multi-element metasurfaces are also essential in antenna applications, lenses, beam splitters, and diffraction gratings, to realize desired far-field patterns.[7]

A common, state-of-the-art practice for synthesizing periodic multi-element metasurfaces is to use a predetermined continuous function of an electromagnetic quantity, which is calculated by an analytical model.[8] The continuous function is discretized, and appropriate unitcells are selected for each position along the metasurface. This process is relatively fast, as only single-unitcell full-wave simulations are needed.[9] However, in certain applications, an analytical distribution may not be available. In such cases, metasurfaces are often synthesized by full-wave simulations of the entire supercell, which are computationally expensive, especially for larger or more complex metasurfaces. Optimized configurations must be

subsequently designed by full-wave-simulation-based optimization, which is even more computationally prohibitive. Hence, there is a need for a significantly faster method that may facilitate and accelerate the design of such complex metasurface structures, while also maintaining high accuracy.

The coupled-mode theory (CMT)[10,11] is a semi-analytical method that has been used to effectively model configurations consisting of a small number of resonators, frequently coupled to one or more transmission lines.[12–15] It has been also extensively used to analyze uniform metasurfaces by modeling the metasurface unitcell.[16–19] Recently, periodic multi-element metasurfaces are also analyzed by the CMT,[20–23] mostly in thermal emitter applications, providing a faster alternative to full-wave simulations. Within the CMT framework, coupling coefficients between the resonators are frequently determined by fitting the CMT curve to full-wave spectral simulations.[22,23] Overlap integrals have also been used in certain cases.[21,24] Analytical models have been used for simple geometric shapes.[21] We also note that radiation losses are inherently present in all microwave free-space devices, such as absorbers, as they quantify the coupling of each resonator mode to the incident wave. It is important to accurately and systematically derive analytical expressions for the coupling coefficients between resonators that also take radiation losses into account, in order to fully capture the underlying physics and provide a systematic path to metasurface design.

In this work, we propose a CMT formulation for the fast and accurate analysis and synthesis of periodic multi-element metasurfaces comprised by weakly coupled resonant elements by systematically deriving closed-form expressions for the coupling coefficients in the presence of radiation losses. The coupling coefficients are straightforwardly and effortlessly determined, instead of using a fitting process, which is a different well-documented approach. The closed-form coupling coefficient expressions will provide greater insight into the underlying physics of complex metasurfaces and facilitate the synthesis of optimized structures. The derived expressions are simple, as they resemble the ones used in lossless systems,[25] and require only knowledge of the coupled and uncoupled complex angular resonance frequencies. The use of eigenfrequency simulations instead of multiple full-wave excitation simulations to determine the coupling coefficients provides an additional side advantage. Our formulation is versatile, as it may be applied to both metal and dielectric resonant metasurfaces,[26] circumventing limitation of other semi-analytical approaches that are based on surface current formulations.[27] We demonstrate the validity of the proposed formulation across different microwave absorber platforms, synthesized by periodic multi-element metal or dielectric resonators. We will thereby compare the CMT response against the response obtained by full-wave spectral simulations of the composing supercell. To further demonstrate the potential of this semi-analytical approach, as proof of concept, we synthesize a larger optimized microwave metasurface absorber (MSA) by using the CMT in conjunction with an optimization algorithm. Finally, we provide a comprehensive discussion on the advantages of the CMT formulation over full-wave synthesis approaches by demonstrating the time benefits on a complex, three-dimensional, computationally challenging microwave absorber metasurface.

II. CMT FORMULATION FOR N WEAKLY COUPLED RESONATORS

We consider a metasurface consisting of N weakly coupled resonators, excited by a normally incident plane wave. In this work, we consider periodic multi-element metasurfaces, with the resonator pattern arranged on a metal-backed substrate; hence, a single port exists. Within the CMT framework, each resonator mode is described by a decay rate equation, with the entire metasurface modeled as follows,[11] assuming a time harmonic convention of $\exp(j\omega t)$,

$$\frac{d\mathbf{A}(t)}{dt} = j\mathbf{\Omega_0}\,\mathbf{A}(t) - \mathbf{\Gamma_e}\,\mathbf{A}(t) - \mathbf{\Gamma_i}\,\mathbf{A}(t) + \mathbf{K}^T s^+, \quad (1)$$

with

$$\mathbf{A}(t) = [\alpha_1(t), \alpha_2(t), \ldots, \alpha_N(t)]^T, \quad (2a)$$

$$\mathbf{\Omega_0} = \mathrm{diag}(\omega_{t,1}, \omega_{t,2}, \ldots, \omega_{t,N}), \quad (2b)$$

$$\mathbf{\Gamma_i} = \mathrm{diag}(\gamma_{i,1}, \gamma_{i,2}, \ldots, \gamma_{i,N}), \quad (2c)$$

$$\mathbf{K} = [k_1, k_2, \ldots, k_N], \quad (2d)$$

$$\mathbf{\Gamma_e} = \begin{bmatrix} \gamma_{e,1} & \kappa_{12} & \cdots & \kappa_{1N} \\ \kappa_{21} & \gamma_{e,2} & \cdots & \kappa_{2N} \\ \vdots & \vdots & \ddots & \vdots \\ \kappa_{N1} & \kappa_{N2} & \cdots & \gamma_{e,N} \end{bmatrix}. \quad (2e)$$

The vector $\mathbf{A}(t)$ denotes the resonator mode amplitudes, with $|\alpha_n(t)|^2$ being the energy stored in resonator n. We focus on resonators that support a single mode within the frequency range of interest, with the resonator modes being well-separated. The diagonal matrix $\mathbf{\Omega_0}$ refers to the individual angular resonance frequencies (real part) of all modes, considering any intrinsic loss mechanism present. The diagonal elements of matrix $\mathbf{\Gamma_e}$ are the external decay rates of each resonator mode, and the off-diagonal elements are the total coupling coefficients between resonators, including all near- and far-field coupling effects. Other alternatives are also possible, for instance, assigning near-field coupling effects to the off-diagonal positions of $\mathbf{\Omega_0}$ and exclusively far-field coupling effects to $\mathbf{\Gamma_e}$. In our formulation, we do not opt for distinguishing between near- and far-field coupling effects. The diagonal matrix $\mathbf{\Gamma_i}$ refers to the intrinsic decay rates, s^+ is the amplitude of the incident wave, and vector $\mathbf{K}$ refers to the coupling between every resonator and the incident wave s^+.

The decay-rate system of equations (1) is complemented by an equation that relates the amplitude of the reflected wave s^- to that of the incoming wave s^+ and the resonator mode amplitudes. In addition, c accounts for the direct scattering process in the absence of resonators, which in our case is the return from a fully reflecting metal surface (perfect electric conductor). The quantities c, s^+, and s^- are scalar, as we refer to a single-port configuration. The vector $\mathbf{D} = \begin{bmatrix} d_1 & d_2 & \cdots & d_N \end{bmatrix}$ quantifies the coupling of each mode to

the outgoing wave,

$$s^- = cs^+ + \mathbf{D}A(t). \tag{3}$$

Once the system of equations described in Eq. (1) is solved, in steady-state or under transient illumination, we can calculate the metasurface response by Eq. (3).

By energy conservation, time-reversal symmetry, and reciprocity, the following conditions[11] apply, strictly valid for $\mathbf{\Gamma_i} = \mathbf{0}$:

$$\mathbf{D}^\dagger \mathbf{D} = \mathbf{\Gamma_e}^\dagger + \mathbf{\Gamma_e}, \tag{4a}$$

$$c\mathbf{D}^* = -\mathbf{D}, \tag{4b}$$

$$\mathbf{K} = \mathbf{D}, \tag{4c}$$

where $\dagger$ denotes the conjugate transpose of the matrix. We note that we use the condition of Eq. (4a) instead of $\mathbf{D}^\dagger \mathbf{D} = 2\mathbf{\Gamma_e}$,[11] as in our case, $\mathbf{\Gamma_e}$ is not Hermitian, with the off-diagonal terms accommodating all coupling interactions, far-field and near-field. A similar approach is also adopted in other relevant recent publications of the literature, such as Refs. 23 and 28, if one groups near- and far-field coupling effects in a single matrix.

The restriction imposed by Eq. (4a) translates as follows for all diagonal and off-diagonal elements:

$$|d_n| = \sqrt{2\gamma_{e,n}}, \tag{5a}$$

$$\kappa_{mn}^* + \kappa_{nm} = d_m d_n^*, \quad n \neq m, \tag{5b}$$

with $n, m = 1, 2, \ldots, N$. By Eq. (4b) and by expressing c and d_n as $c = |c|\, e^{j\phi_c}$ and $d_n = |d_n|\, e^{j\phi_{d,n}}$, we derive the following restriction:

$$\phi_{d,n} = \frac{\phi_c \pm \pi}{2}. \tag{6}$$

We continue with $\phi_{d,n} = (\phi_c - \pi)/2$, noting that equivalent results are also obtained with other sign selection, provided that minor adjustments are made to the subsequent equations. Hence, the off-diagonal elements of Eq. (5b) are written as

$$\kappa_{mn}^* + \kappa_{nm} = |d_n||d_m|, \quad n, m = 1, 2, \ldots, N, \tag{7}$$

as d_m and d_n are in phase. We note that we exclusively consider normally incident plane waves as excitation. For oblique incidence, d_m and d_n would have to acquire a phase difference related to the angle of incidence, the distance between resonators m and n, and the operating wavelength.[28] The aforementioned restrictions will be also used in the upcoming section to derive the coupling coefficients κ_{mn} and κ_{nm}.

III. COUPLING BETWEEN RESONATORS IN THE PRESENCE OF RADIATION LOSSES

To form the system of equations described in Eq. (1), we must calculate the resonator parameters, i.e., the resonance frequencies

and decay rates (intrinsic and external) as well as the coupling coefficients between resonators. To calculate these parameters, we conduct single-resonator and pairwise FEM eigenfrequency simulations. In all FEM eigenfrequency simulations, radiation losses are inherently present for metasurfaces that couple to an normally incident plane wave. In Ref. 25, the coupling coefficients are derived for the case of two lossless resonators; hence, they assume purely imaginary values $\kappa_{mn} = j|\kappa_{mn}|$, $\kappa_{nm} = j|\kappa_{nm}|$ and quantify the frequency splitting that occurs due to coupling. In this work, we will derive generalized coupling coefficient expressions that include the contribution of the inherent radiation losses.

To that end, we consider two weakly coupled resonators in the presence of radiation losses and form the CMT system of equations described in Sec. II by Eqs. (1)–(7). In Ref. 25, the CMT equations are derived by assuming weak coupling between the resonators, i.e., $|\kappa_{12}| \ll \omega_1$ and $|\kappa_{21}| \ll \omega_2$. Under weak coupling, the time dependence is only weakly perturbed, and coupling will affect time evolution when the uncoupled resonant frequencies are close to each other.[25,29] Under these conditions, the coupling terms can be introduced as in Eq. (1), in the form of $\kappa_{mn}A_n$, with high accuracy. We note that weak coupling is related to the form of coupled equations and not the coupling coefficient calculation method, frequency regime, or intended application. Our approach is applicable to the same range of coupling coefficient values, as compared to those of relevant references,[21,23,28] thus being appropriate to describe the same level of resonator interaction. Equation (7) now reads $\kappa_{21}^* + \kappa_{12} = |d_1||d_2|$, leading to the following restrictions on the real and imaginary parts of the coupling coefficients:

$$\Re\{\kappa_{21}\} + \Re\{\kappa_{12}\} = |d_1||d_2|, \tag{8a}$$

$$\Im\{\kappa_{12}\} = \Im\{\kappa_{21}\}. \tag{8b}$$

We observe that κ_{12} and κ_{21} have equal imaginary parts, whereas the real parts are not necessarily equal. We note that if the resonators have no radiation losses, $|d_1||d_2|$ would be equal to zero, and then the restriction imposed in Ref. 25 would be satisfied, $\Re\{\kappa_{21}\} = -\Re\{\kappa_{12}\}$ and $\Im\{\kappa_{12}\} = \Im\{\kappa_{21}\}$, i.e., $\kappa_{21} = -\kappa_{12}^*$. The restriction $\kappa_{21} = -\kappa_{12}^*$ is valid for purely imaginary coupling coefficients as well.

As a next step, we revisit Eq. (1) for the case of two weakly coupled resonators with only radiation losses included and set the incident wave s^+ equal to zero. We highlight that even though our full system described by Eq. (1) is lossy, with only Eq. (4c) valid among Eqs. (4a)–(4c), the deduction of the coupling coefficients in our analysis is based on the auxiliary problem of pairwise coupled resonators with intrinsic losses switched-off, for which all Eqs. (4a)–(4c) apply. We form the system matrix and set its determinant to zero to extract the natural frequencies of the coupled system and obtain a non-trivial solution,[25]

$$\left| \begin{bmatrix} j(\omega - \omega_{e,1}) + \gamma_{e,1} & \kappa_{12} \\ \kappa_{21} & j(\omega - \omega_{e,2}) + \gamma_{e,2} \end{bmatrix} \right| = 0, \tag{9}$$

where $\omega_{e,n}$ are the angular resonance frequencies assuming only external losses. A polynomial of second order in terms of the

angular frequency ω is obtained,

$$\omega^2 - H\omega - G = 0, \tag{10}$$

with $\quad G = -\omega_{e,1}\omega_{e,2} + \gamma_{e,1}\gamma_{e,2} - \kappa_{12}\kappa_{21} - j\omega_{e,1}\gamma_{e,2} - j\omega_{e,2}\gamma_{e,1} \quad$ and $H = \omega_{e,2} + \omega_{e,1} + j\gamma_{e,1} + j\gamma_{e,2}$. The coupled angular frequencies (ω_c^+ and ω_c^-) are derived in terms of the uncoupled frequencies, the decay rates of the uncoupled resonators, and the coupling coefficients by Eqs. (11a) and (11b),

$$2\omega_c^+ = H + \sqrt{\Delta}, \tag{11a}$$

$$2\omega_c^- = H - \sqrt{\Delta}, \tag{11b}$$

with $\Delta = H^2 + 4G$ being the discriminant. We subtract Eq. (11b) from Eq. (11a) and solve for the product of the coupling coefficients $\kappa_{12}\kappa_{21}$,

$$\kappa_{12}\kappa_{21} = \left(\frac{\Delta\omega_u}{2}\right)^2 - \left(\frac{\Delta\omega_c}{2}\right)^2, \tag{12}$$

with $\Delta\omega_u = (\omega_{e,1} + j\gamma_{e,1}) - (\omega_{e,2} + j\gamma_{e,2})$ and $\Delta\omega_c = \omega_c^+ - \omega_c^-$. We note that the coupled angular frequencies ω_c^+, ω_c^- are complex. This equation is similar to the one derived in Ref. 25, with the critical addition of the external decay rate terms of each uncoupled resonator to account for radiation losses. The coupling coefficients are also complex, with the real part related to radiation losses.

By using Eqs. (8a) and (8b), the left side of Eq. (12) is written as $-\Re\{\kappa_{12}\}^2 - L\Re\{\kappa_{12}\} - \Im^2\{\kappa_{12}\} - j\Im\{\kappa_{12}\}L$, with $L = -|d_1\|d_2|$. By equating the real and imaginary parts of Eq. (12), two equations are formed. The equation related to the imaginary part dictates that the imaginary part of κ_{12} is equal to

$$\Im\{\kappa_{12}\} = -\Im\left\{\left(\frac{\Delta\omega_u}{2}\right)^2 - \left(\frac{\Delta\omega_c}{2}\right)^2\right\}\bigg/ L. \tag{13}$$

The equation related to the real part is a second-order polynomial in terms of $\Re\{\kappa_{12}\}$,

$$\Re\{\kappa_{12}\}^2 + L\Re\{\kappa_{12}\} + F = 0, \tag{14}$$

with

$$F = \Im^2\{\kappa_{12}\} + \Re\left\{\left(\frac{\Delta\omega_u}{2}\right)^2 - \left(\frac{\Delta\omega_c}{2}\right)^2\right\}. \tag{15}$$

The roots of Eq. (14) are the real parts of κ_{12} and κ_{21}. Since Eq. (8a) was used to derive Eq. (14), by setting $\Re\{\kappa_{12}\}$ equal to either of the two roots of Eq. (14), $\Re\{\kappa_{21}\}$, can be equivalently determined either as the other root of Eq. (14) or by applying Eq. (8a). We note that $\Re\{\kappa_{12}\}$ and $\Re\{\kappa_{21}\}$ are interchangable, leading to the same CMT response, as the outgoing wave of Eq. (3) exclusively involves the sum $\kappa_{12} + \kappa_{21}$ and product $\kappa_{12}\kappa_{21}$. Equations (14) and (13) provide closed-form expressions to

determine the real and imaginary parts of the coupling coefficients of a pair of weakly coupled resonators.

IV. CALCULATION OF RESONATOR PARAMETERS

A. Single-resonator parameters: Intrinsic and external Q-factors and decay rates

We carry out single-resonator eigenfrequency FEM simulations to determine the intrinsic and external resonator parameters that feed Eq. (1). The external decay rate is calculated by switching off the intrinsic losses; hence, only radiation (external) losses remain. To that end, we impose perfect electric conductor (PEC) boundary conditions on all metal surfaces and assign a real value to the dielectric constant. The intrinsic resonator parameters cannot be directly calculated by an eigenfrequency FEM simulation, as the external losses cannot be artificially switched off. For this purpose, we first calculate the total Q-factor, including all loss mechanisms, i.e., dielectric, conductor, and external losses. Conductor losses are considered on the metal resonators by substituting the PEC boundary conditions with transition boundary conditions (TBCs) to model the finite metal conductivity. Periodic boundary conditions (PBCs) are imposed on all side boundaries to model the infinite periodic arrangement. The external ($Q_{e,n}$) and total ($Q_{t,n}$) Q-factors are calculated as[30]

$$Q_{e/t,n} = \frac{\Re(\omega_{e/t,n})}{2\Im(\omega_{e/t,n})}. \tag{16}$$

The external ($\gamma_{e,n}$) and total ($\gamma_{t,n}$) decay rates are then calculated as

$$\gamma_{e/t,n} = \frac{\Re(\omega_{e/t,n})}{2Q_{e/t,n}}. \tag{17}$$

The intrinsic decay rate ($\gamma_{i,n}$), attributed only to conductor and dielectric losses, is retrieved from the total and external decay rates as

$$\frac{1}{\gamma_{i,n}} = \frac{1}{\gamma_{t,n}} - \frac{1}{\gamma_{e,n}}. \tag{18}$$

The external and intrinsic decay rates and resonance frequencies are calculated for each resonator type and will be used to feed the CMT system of equations and subsequently calculate the metasurface response.

B. Coupling coefficients

We will examine the effect of resonator coupling by considering benchmark examples of metal- and dielectric-based resonator pairs. To apply Eqs. (14) and (13), we determine the coupled angular frequencies, ω_c^+ and ω_c^-, by pairwise eigenfrequency FEM simulations with only external losses included. The computational layout is identical to the single-resonator eigenfrequency simulation.

We first consider a split-ring-resonator (SRR) MSA, with two SRRs of radii $r_1 = 1.475\text{ mm}$ and $r_2 = 1.525\text{ mm}$, oriented along the x-axis and separated by a distance of D_x. The SRR MSA is arranged on a PEC-backed FR4 dielectric substrate of thickness $h = 1.6\text{ mm}$ and $\varepsilon_r = 4.3(1 - j0.025)$. The SRR ring width is
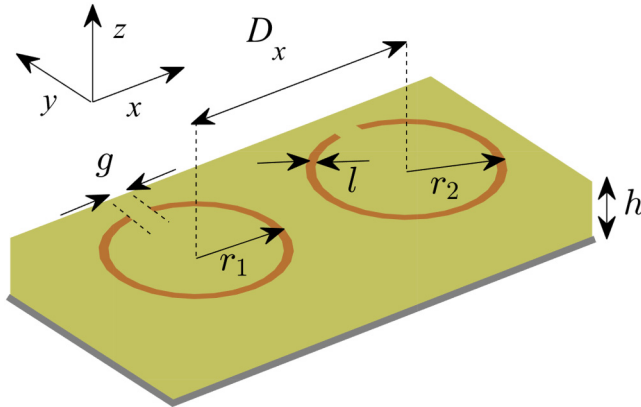
FIG. 1. 3D schematic of the 2 × 1 horizontally placed SRR-MSA. D_x is the distance between the centers of the two SRRs.

$l = 0.3$ mm and the gap is $g = 0.4$ mm. A 3D schematic of the SRR MSA is shown in Fig. 1, along the main SRR geometric features.

We vary the distance D_x between the SRRs in the range $D_x = [3.5, 5.2]$ mm and calculate the coupling coefficients κ_{12} and κ_{21} by Eqs. (15) and (13). The real and imaginary parts of κ_{12} are

plotted in Fig. 2(a), varying the distance D_x. In this example, $\Re\{\kappa_{12}\} \approx \Re\{\kappa_{21}\}$; hence, we plot only $\Re\{\kappa_{12}\}$. We observe that, the real part of the coupling coefficient, which quantifies radiation losses, gradually decreases as the distance between the SRRs increases, experiencing small changes of about 0.6 GHz among the largest and smallest distance. The imaginary part experiences greater variation. As the distance increases, the imaginary part also decreases, with the imaginary part at $D_x = 5.2$ mm being about one-eighth of the corresponding value at $D_x = 3.5$ mm.

The coupling of SRRs depends not only on the distance between them but also on their relative orientation. Hence, we consider a different orientation of the two SRRs by placing them along the y-axis at distance D_y, with the other geometric parameters retained, as shown in the inset of Fig. 2(b). The real and imaginary parts of the coupling coefficient κ_{12} are also plotted in Fig. 2(b) by varying D_y in the same range. In this case, it is $\Re\{\kappa_{12}\} \approx \Re\{\kappa_{21}\}$ similar to the previous orientation. We observe that the imaginary part assumes considerably lower values than those of the horizontally placed SRRs; hence, vertical orientation results in weaker coupling, which is anticipated for this SRR orientation. At the distance $D_y = D_x = 4$ mm, the vertically placed SRRs experience weaker coupling by a factor close to five. The real parts are similar in both cases.

To show the versatility of our approach, we also consider a benchmark example of two high-index dielectric-cube resonators of relative permittivity $\varepsilon_r = 115 - j0.92$ arranged on a PEC plate,
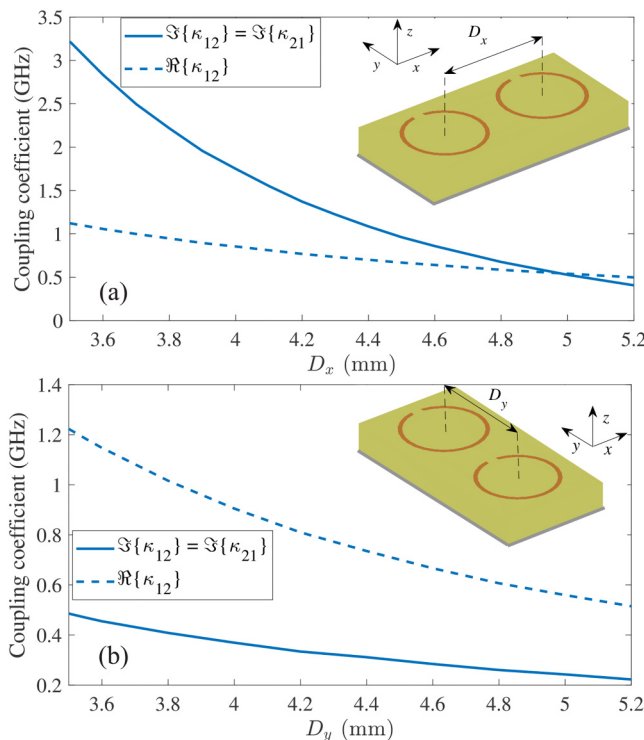

FIG. 2. Real and imaginary parts of the coupling coefficient vs the distance (a) D_x and (b) D_y for a 2 × 1 (a) horizontally and (b) vertically placed SRR-MSA.
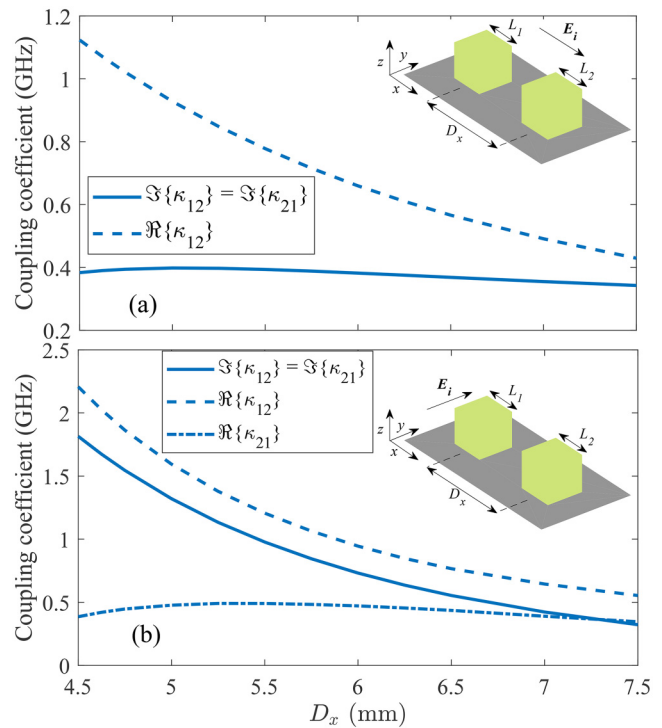

FIG. 3. Real and imaginary part of the coupling coefficient vs the distance D_x for a 2 × 1 dielectric-cube MSA with the (a) x- and (b) y-polarization-excited coupled-resonator mode.

08 January 2024 13:05:13

acting as isotropic Mie-based MSAs.[31] The dielectric cubes are embedded in a $2D_x \times D_x$ environment, separated by distance D_x, and are of side length $L_1 = 2$ mm and $L_2 = 2.1$ mm, shown as insets in Fig. 3. Two sets of modes are supported in a system of two coupled dielectric cubes, each excited by an x- and y-polarized incident wave, respectively. We calculate the coupling coefficient for each case, vary D_x between 4.5 and 7.5 mm, and plot the real and imaginary parts in Figs. 3(a) and 3(b). We observe that the imaginary part of the coupling coefficient is considerably stronger for y-polarization coupled-mode, while it remains almost constant for x-polarization. We also note that while the real parts of κ_{12} and κ_{21} are equal to each other for x polarization, they do not coincide in the case of y polarization, albeit both satisfy the relation $\Re\{\kappa_{12}\} + \Re\{\kappa_{21}\} = |d_1\|d_2|$.

V. VALIDATION OF THE CMT FRAMEWORK

We validate the proposed framework by using the CMT to calculate the response of certain benchmark examples. We consider the SRR and dielectric-cube MSA of Sec. IV and compare the CMT results to FEM spectral simulations of the entire supercell. We also consider a 4×1 periodic multi-element SRR MSA to demonstrate the extensibility of our formulation toward larger and more complex configurations, where not all resonators are first-nearest neighbors. In all cases, $|\kappa_{12}|$ is roughly two orders of magnitude below ω_1 and ω_2, where the CMT is shown to exhibit high accuracy. In all examples, both the real and imaginary parts of the coupling coefficients are needed to accurately replicate the FEM response.

A. 2 × 1 horizontally placed periodic multi-element SRR MSA

We first consider the horizontally placed SRR MSA with $D_x = 4.8$ mm. The CMT and FEM results are in excellent agreement, as shown in Fig. 4.

B. 2 × 1 vertically placed periodic multi-element SRR MSA

We also validate the CMT results against FEM simulations for the vertically placed SRR MSA with $D_y = 4$ mm. We calculate
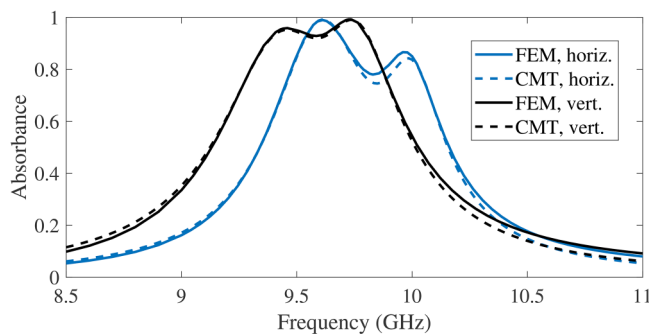

FIG. 4. Absorbance vs frequency of both a 2×1 horizontally and vertically placed SRR-MSA by the CMT and FEM.
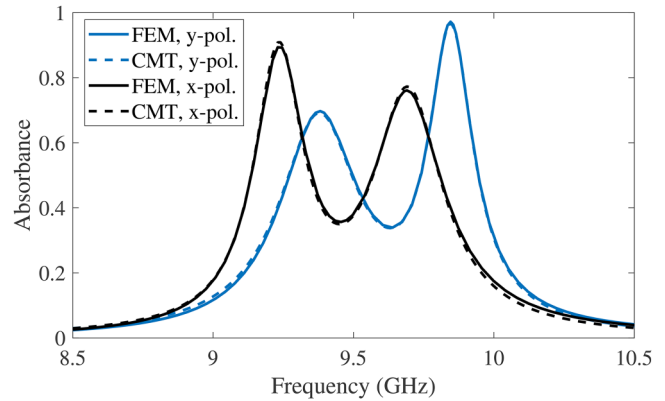

FIG. 5. Absorbance vs frequency of a 2×1 dielectric-cube MSA, via CMT and FEM, for an x- and y-polarized incident wave.

absorbance via CMT and FEM and compare the results in Fig. 4. An excellent agreement is attained with both resonances accurately recovered.

C. 2 × 1 dielectric-cube MSA

As a last validation step, we compare CMT results to FEM simulations of the dielectric-cube MSA, considering $D_x = 6.5$ mm, for both an x- and y-polarized incident wave. An excellent agreement is observed for both polarizations, as shown in Fig. 5.

D. 4 × 1 horizontally placed periodic multi-element SRR MSA

We consider a 4×1 SRR-MSA with all SRRs placed along the x-axis and of radii $[r_1, r_2, r_3, r_4]$, with $r_1 = 1.425$ mm, $r_2 = 1.475$ mm, $r_3 = 1.525$ mm, and $r_4 = 1.425$ mm. In this
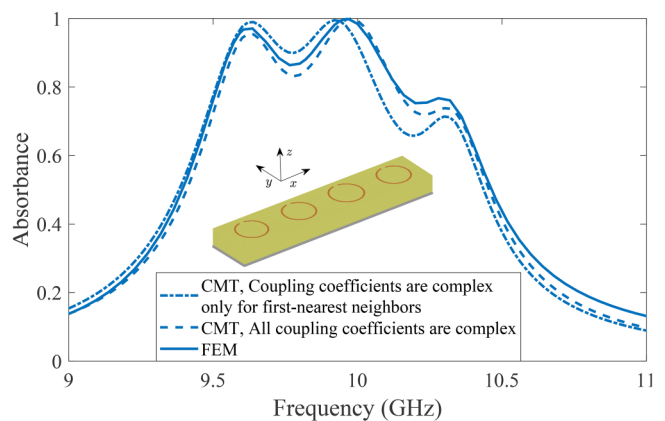

FIG. 6. Absorbance vs frequency for a 4×1 SRR-MSA, calculated by the CMT and FEM.

example, not all resonators are nearest neighbors. We first determine the CMT response by taking into account the coupling between all pairs of resonators, i.e., first-nearest neighbors r_1-r_2, r_2-r_3, r_3-r_4, r_4-r_1 and second nearest neighbors r_1-r_3 and r_2-r_4, with all coupling coefficients assuming complex values. The results are shown in Fig. 6, and an excellent agreement is observed. As a next step, we consider complex coupling coefficients only for the first-nearest neighbors and purely real coupling coefficients for resonators that are placed further apart. The real parts of the coupling coefficients are required for energy-conservation, following Eq. (5b). In this case, the pairwise eigenfrequency simulations are performed only for the first-nearest neighbors. The real part of the coupling coefficients of the remaining pairs is approximated as $|d_m||d_n|/2$, with the required quantities already available by the single-resonator simulations. The expression $|d_m||d_n|/2$ is derived by assuming that κ_{mn} and κ_{nm} are purely real and equal to each other in Eq. (7). In Ref. 21, a similar expression is used for the far-field coupling between resonators m and n, introduced as the off-diagonal terms of the decay rate matrix. We note that in our formulation, the coupling coefficient (and subsequently its real part) incorporates all coupling effects; however, for resonators that are further apart, near-field coupling is expected to be less prominent. We also note that the real parts of the coupling coefficients are not in general equal to each other; hence, equating the real parts of the coupling coefficients may be an additional source of inaccuracy in some cases. The absorbance, which is calculated by assuming complex coupling-coefficient values only for the first-nearest neighbors, is also shown in Fig. 6. A better agreement is observed when all coupling coefficients assume complex values, hence fully accounting for all coupling mechanisms. However, for larger configurations, where performing eigenfrequency simulations across all pairs of resonators may become considerably time-consuming, this alternative approach may provide a faster though approximate result.

VI. SYNTHESIS OF AN OPTIMIZED MSA

The CMT generally offers valuable insight into the working principle of the metasurface and the coupling between resonators. However, CMT may be additionally used as a fast and computationally efficient method to synthesize metasurfaces of a desired functionality. To that end, as a first step, we form a library of the resonator parameters (resonance frequency, external and intrinsic decay rates, and Q-factors) for different types of resonators. Coupling coefficients between all resonator-type combinations are also included in the library. Once the resonator parameters and coupling coefficients are determined, we synthesize the desired metasurface by solving the CMT system of equations for different parameter sets. An optimized configuration is obtained by combining the CMT solver with an optimization algorithm.

We consider a 2×3 SRR-MSA supercell, with two and three SRRs oriented along the x- and y-axis, respectively. The 2×3 SRR MSA is used to highlight the benefits of our formulation within a more complex and realistic test case. We let the SRRs assume three distinct values $r_1 = 1.475$ mm, $r_2 = 1.525$ mm, and $r_1 = 1.575$ mm with the ring width and the SRR gap retained. We first validate the CMT by analyzing an arbitrary 2×3 configuration and compare it
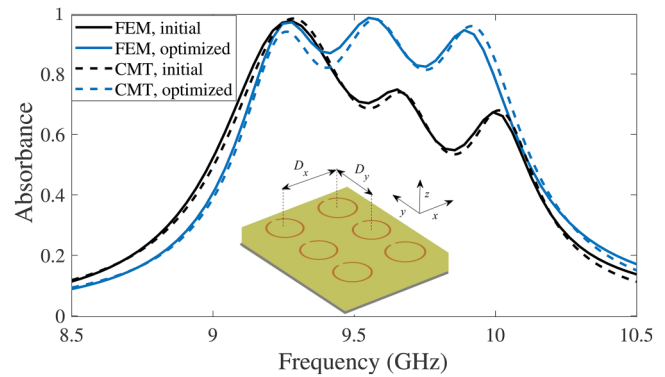

FIG. 7. Absorbance vs frequency for a 2×3 SRR-MSA, calculated by the CMT and FEM. Both the initial arbitrary and the optimized configurations are included.

to full-wave simulations of the entire supercell. The arbitrary configuration layout is as follows:

$$L_i = \begin{bmatrix} r_3 & r_1 \\ r_2 & r_3 \\ r_3 & r_3 \end{bmatrix}. \tag{19}$$

As a next step, we obtain an optimized layout by combining genetic-algorithm optimization with the CMT solver. The design objective is to maximize the absorbance over the largest attainable bandwidth. We set the minimum acceptable absorption level to $A = 0.8$. The optimized configuration layout is as follows:

$$L_o = \begin{bmatrix} r_3 & r_3 \\ r_2 & r_2 \\ r_1 & r_1 \end{bmatrix}, \tag{20}$$

which turns out to be 1×3 MSA. We compare the CMT results of the initial and optimized configurations against the FEM results of the entire supercell (Fig. 7), with an overall very good agreement observed in both cases. The optimized MSA exhibits absorbance higher than $A = 0.8$ over a 0.83 GHz range, whereas the initial design features absorbance $A > 0.8$ in a considerably narrower band of 0.29 GHz. Average absorbance calculations over the 9.1–10.1 GHz band also corroborate that the design obtained by the CMT-based optimization features better performance than the initial one, with the average absorbance of the initial and optimized design being Avg{A_i} = 0.728 and Avg{A_o} = 0.86, respectively.

VII. DISCUSSION ON COMPUTATIONAL REQUIREMENTS

The proposed CMT methodology is a computationally efficient alternative to full-wave simulations for the analysis and synthesis of large-scale metasurfaces. The CMT requires smaller single-resonator and pairwise eigenfrequency simulations to construct the resonator-parameter and coupling-coefficient library. The CMT system of

equations may be then solved very fast for multiple frequencies or different configurations, as the degrees of freedom solved for are extremely low, equal to the number of resonator modes. Full-wave spectral simulations of the entire metasurface supercell, on the other hand, are computationally expensive especially for larger metasurfaces and must be performed multiple times across several frequencies to obtain a spectral response. Hence, full-wave spectral simulations entail not only much higher numbers of DoFs but also a considerably higher number of computationally expensive simulations. Moreover, they must be recomputed without prior knowledge for different arrangements of resonators.

We, therefore, illustrate the advantages of our proposed formulation in terms of time and computational requirements with the following example. The analysis of a 2×3 MSA configuration, synthesized by three different in size resonators, requires six single-resonator eigenfrequency simulations, three with only external losses and three with all losses included. Each single-resonator eigenfrequency simulation needs about 800 000 degrees of freedom (DoFs) for these specific problems. We also form three coupling-coefficient matrices, each quantifying the coupling between resonator types, oriented along the x ($\boldsymbol{\kappa_x}$), y ($\boldsymbol{\kappa_y}$) and diagonal direction ($\boldsymbol{\kappa_d}$) for the considered configuration. Each coupling-coefficient matrix is of dimensions 3×3 since we consider three different-in-size SRRs to synthesize the MSA. To fill these coupling-coefficient matrices, for each pair of resonator types i and j and for each relative orientation, we perform a pairwise eigenfrequency simulation and obtain the coupling-coefficient matrix elements $\boldsymbol{\kappa_{x/y/d}}(i, j)$ by Eqs. (13)–(15). The κ_{mn} elements of matrix $\boldsymbol{\Gamma_e}$ will be filled using matrices $\boldsymbol{\kappa_{x/y/d}}$ according to the type and orientation of the resonators. The κ_{nm} elements of matrix $\boldsymbol{\Gamma_e}$ in all cases satisfy Eqs. (8a) and (8b). Each 3×3 coupling-coefficient matrix requires up to nine pairwise eigenfrequency simulations, depending on the structure's symmetry. By performing up to 27 pairwise eigenfrequency simulations (nine for each orientation), with each simulation having about 870 000 DoFs, we form the library for this example. Each single-resonator and pairwise eigenfrequency simulation requires 3 min on a high-end XEON server. Once the library set is obtained, the CMT system of equations is solved in less than a second for each metasurface layout. For the example under consideration, the computation of all CMT parameters requires about 1.65 h. A full-wave solver needs about 1 150 000 DoFs and 6 min for a single-frequency calculation; thus, it will require about 5 h to compute the spectral response of a given 2×3 MSA layout across 50 frequencies. The advantages of our formulation are even more evident during the synthesis process. The optimized configuration was obtained via the CMT-based optimization after 30 iterations, as the average relative change in the penalty fitness value was less than 10^{-10}. The CMT needs a few seconds to perform all iterations, provided the 1.65-h overhead, whereas the full-wave FEM solver would need about 6 days. As the size and set of available resonators increase, the full-wave FEM simulations are expected to become prohibitive. Hence, the CMT solver provides a valuable and time-efficient semi-analytical tool that may be used in conjunction with any optimization algorithm for the fast synthesis of metasurfaces.

VIII. CONCLUSION

We proposed a CMT formulation for the fast analysis and synthesis of metasurface structures. Instead of simulating the entire metasurface supercell by a full-wave solver, we construct a small system of equations, one for each resonator mode, fed by simpler and faster single-resonator and pairwise eigenfrequency simulations. As radiation losses are inherent in many practical applications, we derive closed-form expressions for the coupling coefficients between two weakly coupled resonators by properly considering radiation losses. Such analytical expressions may also provide greater insight into the underlying physics. We validated our formulation across different absorber configurations and synthesized an optimized larger microwave absorber to demonstrate the benefits of the CMT on a computationally challenging example. Our method offers a fast, computationally efficient, and accurate tool for synthesizing metasurfaces and may be extended toward two-port or multi-port applications, such as polarization converters, which would require two ports for a metal-backed reflective metasurface (one for the TE and one for TM polarization) and four ports for a non metal-backed transmissive metasurfaces.

AUTHOR DECLARATIONS
Conflict of Interest

The authors have no conflicts to disclose.

Author Contributions

Maria-Thaleia Passia: Conceptualization (lead); Data curation (lead); Formal analysis (lead); Investigation (lead); Methodology (lead); Validation (lead); Visualization (lead); Writing – original draft (lead). **Traianos V. Yioultsis:** Conceptualization (equal); Formal analysis (equal); Investigation (equal); Methodology (equal); Resources (equal); Supervision (equal); Validation (equal); Writing – review & editing (equal). **Emmanouil E. Kriezis:** Conceptualization (equal); Formal analysis (equal); Investigation (equal); Methodology (equal); Resources (equal); Supervision (equal); Validation (equal); Writing – review & editing (equal).

DATA AVAILABILITY

The data that support the findings of this study are available from the corresponding author upon reasonable request.

REFERENCES

[1]C. Caloz and T. Itoh, *Electromagnetic Metamaterials: Transmission Line Theory and Microwave Applications* (John Wiley & Sons, Inc., 2005).
[2]C. L. Holloway, E. F. Kuester, C. A. Gordon, J. O'Hara, J. Booth, and D. R. Smith, "An overview of the theory and applications of metasurfaces: The two-dimensional equivalents of metamaterials," IEEE Antennas Propag. Mag. **54**, 10–35 (2012).
[3]N. I. Landy, S. Sajuyigbe, J. J. Mock, D. R. Smith, and W. J. Padilla, "Perfect metamaterial absorber," Phys. Rev. Lett. **100**, 207402 (2008).
[4]W. Guo, Y. Liu, and T. Han, "Ultra-broadband infrared metasurface absorber," Opt. Express **24**, 20586–20592 (2016).
[5]T. M. Kollatou, A. I. Dimitriadis, S. D. Assimonis, N. V. Kantartzis, and C. S. Antonopoulos, "Multi-band, highly absorbing, microwave metamaterial structures," Appl. Phys. A **115**, 555–561 (2014).
[6]H. Wang and L. Wang, "Perfect selective metamaterial solar absorbers," Opt. Express **21**, A1078–A1093 (2013).

[7]M. Faenzi, G. Minatti, D. Gonzalez-Ovejero, F. Caminita, E. Martini, C. Della Giovampaola, and S. Maci, "Metasurface antennas: New models, applications and realizations," Sci. Rep. **9**, 10178 (2019).

[8]S. Pandi, C. A. Balanis, and C. R. Birtcher, "Design of scalar impedance holographic metasurfaces for antenna beam formation with desired polarization," IEEE Trans. Antennas Propag. **63**, 3016–3024 (2015).

[9]F. Liu, O. Tsilipakos, A. Pitilakis, A. C. Tasolamprou, M. S. Mirmoosa, N. V. Kantartzis, D.-H. Kwon, J. Georgiou, K. Kossifos, M. A. Antoniades, M. Kafesaki, C. Soukoulis, and S. A. Tretyakov, "Intelligent metasurfaces with continuously tunable local surface impedance for multiple reconfigurable functions," Phys. Rev. Appl. **11**, 044024 (2019).

[10]S. Fan, W. Suh, and J. Joannopoulos, "Temporal coupled-mode theory for the Fano resonance in optical resonators," J. Opt. Soc. Am. A **20**, 569–572 (2003).

[11]W. Suh, Z. Wang, and S. Fan, "Temporal coupled-mode theory and the presence of non-orthogonal modes in lossless multimode cavities," IEEE J. Quantum Electron. **40**, 1511–1518 (2004).

[12]L. Zhu, S. Sandhu, C. Otey, S. Fan, M. B. Sinclair, and T. Luk, "Temporal coupled mode theory for thermal emission from a single thermal emitter supporting either a single mode or an orthogonal set of modes," Appl. Phys. Lett. **102**, 103104 (2013).

[13]D. Ketzaki, O. Tsilipakos, T. Yioultsis, and E. Kriezis, "Electromagnetically induced transparency with hybrid silicon-plasmonic traveling-wave resonators," J. Appl. Phys. **114**, 113107 (2013).

[14]T. Christopoulos, O. Tsilipakos, N. Grivas, and E. Kriezis, "Coupled-mode-theory framework for nonlinear resonators comprising graphene," Phys. Rev. E **94**, 062219 (2016).

[15]T. Christopoulos, V. Ataloglou, and E. Kriezis, "All-optical nanophotonic resonant element for switching and routing applications exploiting graphene saturable absorption," J. Appl. Phys. **127**, 223102 (2020).

[16]G. Isić, G. Sinatkas, D. C. Zografopoulos, B. Vasić, A. Ferraro, R. Beccherelli, E. E. Kriezis, and M. Belić, "Electrically tunable metal–semiconductor–metal terahertz metasurface modulators," IEEE J. Sel. Top. Quantum Electron. **25**, 8500108 (2019).

[17]J. R. Piper and S. Fan, "Total absorption in a graphene monolayer in the optical regime by critical coupling with a photonic crystal guided resonance," ACS Photonics **1**, 347–353 (2014).

[18]J. Song, H. Heo, S. Lee, and S. Kim, "Mirror-less unidirectional radiation in an asymmetric single resonator," J. Light Technol. **40**, 5163–5170 (2022).

[19]H. Li, G. Wei, H. Zhou, H. Xiao, M. Qin, S. Xia, and F. Wu, "Polarization-independent near-infrared superabsorption in transition metal dichalcogenide Huygens metasurfaces by degenerate critical coupling," Phys. Rev. B **105**, 165305 (2022).

[20]M.-T. Passia and T. V. Yioultsis, "Fast analysis of metasurfaces through temporal coupled-mode theory," IEEE Trans. Magn. **56**, 7506804 (2020).

[21]M. Zhou, D. Liu, S. W. Belling, H. Cheng, M. Kats, S. Fan, M. L. Povinelli, and Z. Yu, "Inverse design of metasurfaces based on coupled-mode theory and adjoint optimization," ACS Photonics **8**, 2265–2273 (2021).

[22]X. Huang, C. Yeung, and A. P. Raman, "Temporal coupled-mode theory for thermal emission from multiple arbitrarily coupled resonators," Phys. Rev. Appl. **19**, 034037 (2023).

[23]R. Audhkhasi, B. Zhao, S. Fan, Z. Yu, and M. L. Povinelli, "Spectral emissivity modeling in multi-resonant systems using coupled-mode theory," Opt. Express **30**, 9463–9472 (2022).

[24]M. Popović, C. Manolatou, and M. Watts, "Coupling-induced resonance frequency shifts in coupled dielectric multi-cavity filters," Opt. Express **14**, 1208–1222 (2006).

[25]H. A. Haus, *Waves and Fields in Optoelectronics*, Prentice-Hall Series in Solid State Physical Electronics (Prentice-Hall, Englewood Cliffs, NJ, 1984).

[26]X. Liu, C. Lan, K. Bi, B. Li, Q. Zhao, and J. Zhou, "Dual band metamaterial perfect absorber based on Mie resonances," Appl. Phys. Lett. **109**, 062902 (2016).

[27]S. I. Raptis, K. Ntokos, M.-T. Passia, K. Tourlouki, N. Kehagias, E. E. Kriezis, and T. V. Yioultsis, "Ultra-thin and flexible microwave metasurface absorbers based on resistive patches," IEEE Trans. Antennas Propag. (to be published).

[28]L. Verslegers, Z. Yu, P. Ruan, Z. Catrysse, and S. Fan, "From electromagnetically induced transparency to superscattering with a single structure: A coupled-mode theory for doubly resonant structures," Phys. Rev. Lett. **108**, 083902 (2012).

[29]H. Haus and W. Huang, "Coupled-mode theory," Proc. IEEE **19**, 1505–1518 (1991).

[30]T. Christopoulos, O. Tsilipakos, G. Sinatkas, and E. Kriezis, "On the calculation of the quality factor in contemporary photonic resonant structures," Opt. Express **27**, 14505–14522 (2019).

[31]X. Liu, Q. Zhao, C. Lan, and J. Zhou, "Isotropic Mie resonance-based metamaterial perfect absorber," Appl. Phys. Lett. **103**, 031910 (2013).

08 January 2024 13:05:13